

WHY NOT PUT A MICROPHONE NEAR THE LOUDSPEAKER? A NEW PARADIGM FOR ACOUSTIC ECHO CANCELLATION

Fei Zhao^{1,2} and Zhong-Qiu Wang²

¹Inner Mongolia University, China

²Southern University of Science and Technology, China

zhaofei@mail.imu.edu.cn, wang.zhongqiu41@gmail.com

ABSTRACT

Acoustic echo cancellation (AEC) remains challenging in real-world environments due to nonlinear distortions caused by low-cost loudspeakers and complex room acoustics. To mitigate these issues, we introduce a dual-microphone configuration, where an auxiliary reference microphone is placed near the loudspeaker to capture the nonlinearly distorted far-end signal. Although this reference signal is contaminated by near-end speech, we propose a preprocessing module based on Wiener filtering to estimate a compressed time-frequency mask to suppress near-end components. This purified reference signal enables a more effective linear AEC stage, whose residual error signal is then fed to a deep neural network for joint residual echo and noise suppression. Evaluation results show that our method outperforms baseline approaches on matched test sets. To evaluate its robustness under strong nonlinearities, we further test it on a mismatched dataset and observe that it achieves substantial performance gains. These results demonstrate its effectiveness in practical scenarios where the nonlinear distortions are typically unknown.

Index Terms— acoustic echo cancellation, auxiliary reference microphone, short-time Wiener filtering

1. INTRODUCTION

Acoustic echo cancellation (AEC) is a critical signal processing task that aims to remove undesired echo signals caused by acoustic coupling between loudspeakers and microphones in voice communication systems [1,2]. Traditional AEC methods primarily rely on adaptive filtering [3–5], such as NLMS and PBFDAF, which achieve robust performance across varying acoustic conditions through online adaptation. However, these linear models are inherently limited in handling nonlinear distortions [6,7], especially when low-cost audio hardware introduces harmonic artifacts or clipping. This limitation leads to persistent residual echo, degrading user experience in real-world deployments.

To address these limitations, deep learning-based AEC methods have emerged and can be broadly categorized into three paradigms: **1) End-to-End Deep Neural Networks (DNN)**: These models learn a direct mapping from microphone signals to echo-canceled outputs using strong deep architectures [8–11]. While achieving state-of-the-art performance on in-distribution data, they exhibit limited generalizability to unseen acoustic environments and nonlinear distortions [12–14]. **2) Cascaded Traditional-Neural Systems**: This hybrid approach first applies conventional adaptive filtering for coarse

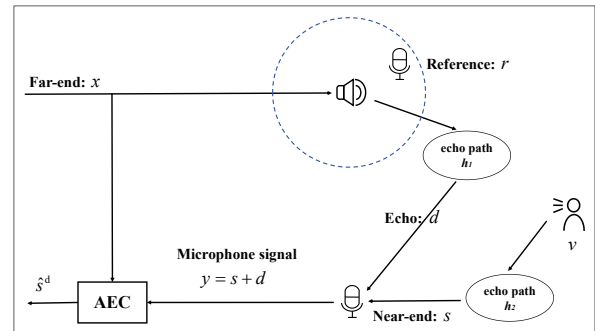


Fig. 1: Illustration of AEC aided by using an auxiliary reference microphone.

echo suppression, followed by DNNs for residual echo removal [15–18]. Although it reduces training complexity and improves overall performance, the DNN’s generalizability remains a bottleneck. **3) Neural-Adaptive Hybrid Methods**, where DNNs are trained to predict the parameters for adaptive filters [19–21] (e.g., step sizes, regularization weights). Such methods inherit the generalization benefits of traditional AEC but often underperform purely data-driven or cascaded systems in terms of absolute echo suppression [20].

Nonlinear distortions in AEC systems typically originate from loudspeaker and amplifier characteristics, such as hard clipping, sigmoid-like amplitude responses, and amplifier saturation. These phenomena introduce harmonic and inter-modulation distortion. Additionally, excessive mechanical vibrations from high-intensity signals can induce further nonlinearities due to structural resonance or driver instability [22].

To address the prominent non-linearity challenge in AEC, we propose a microphone-augmented solution. As shown in Fig. 1, an auxiliary reference microphone is placed near the loudspeaker in a conventional AEC system to capture nonlinearly distorted far-end reference signal. Prior work has explored multi-microphone AEC [10], but typically uses distant compact microphone arrays for spatial filtering. In contrast, the recorded reference signal contains the non-linearly distorted far-end signal, and could mitigate the difficulties in AEC caused by unknown non-linear distortions. However, the reference signal also contains non-negligible near-end signals, which would interfere with nonlinearity-focused processing. To suppress the near-end signals, we employ a two-stage preprocessing pipeline: a short-time Wiener filter is first applied between the far-end and reference signals to estimate the far-end components, followed by computing an ideal ratio mask (IRM) to suppress the near-end components. This yields a purified reference signal. Subsequently, the far-end signal, original reference signal, and purified reference signal are jointly processed with the main microphone signal using Wiener filtering for preliminary echo suppression. Finally, all signals are fed

This work was done while Fei Zhao was a visiting student at SUSTech. Corresponding author: Zhong-Qiu Wang.

into the AEC model to predict the near-end direct signal. Our evaluation results show that this method not only achieves significant performance gains over baseline systems but also exhibits superior robustness, particularly under strong, unseen nonlinear distortions such as clipping and amplifier saturation, confirming its effectiveness in practical scenarios.

2. PROBLEM FORMULATION

Fig. 1 shows our proposed single-channel AEC system, which features an auxiliary reference microphone positioned in proximity to the loudspeaker. This strategic placement allows it to effectively capture the loudspeaker’s nonlinear output. Assuming weak ambient noise, the mixture signal captured by the main microphone, y , is modeled as a mixture of the acoustic echo signal d and near-end speech signal s . The physical model in the time domain can be expressed as

$$\begin{aligned} y &= v * h_1 + x_{nl} * h_2 & (1) \\ &= s + d & (2) \\ &= s^d + s^r + d \in \mathbb{R}^N, & (3) \end{aligned}$$

where $*$ denotes linear convolution and N signal length in samples. The near-end signal s arises from convolving the anechoic near-end source v with its propagation room impulse response (RIR) h_1 , and decomposes into two physically interpretable components: the direct-path component s^d (unreflected sound from the near-end source to the main microphone) and late reverberant component s^r (multiple late reflections of v within the room). The acoustic echo d , meanwhile, is generated by convolving the loudspeaker’s nonlinear output x_{nl} (a distorted version of the far-end signal x) with the echo-path RIR h_2 .

The mixture signal captured by the auxiliary reference microphone, r , is a composite of the far-end signal component, r^f , and the contaminating near-end signal, r^n , formulated as:

$$\begin{aligned} r &= v * h_3 + x_{nl} * h_4 & (4) \\ &= r^n + r^f, & (5) \end{aligned}$$

where h_3 and h_4 respectively denote the RIRs from the loudspeaker and near-end talker to the reference microphone. Crucially, due to this microphone’s proximity to the loudspeaker, the far-end component exhibits much larger energy than the near-end component. This large energy disparity is the key physical property we exploit to isolate the nonlinear far-end signal for more effective AEC.

3. PROPOSED METHOD

Our proposed system, shown in Fig. 2, operates in the short-time Fourier transform (STFT) domain. It comprises two stages: a linear AEC stage, which suppresses the near-end component in the reference signal and performs signal processing-based linear AEC, and a neural AEC stage suppresses residual echoes.

3.1. Linear AEC Stage

3.1.1. Weighted short-time Wiener solution

For the linear AEC component, we adopt the weighted short-time Wiener solution (WSTWS) [23], an enhancement over the conventional short-time Wiener solution (STWS) [24] by adaptively re-weighting the contribution of individual time-frequency (T-F) units

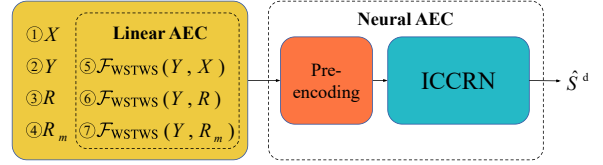


Fig. 2: Architecture of proposed AEC system.

[23]. The linear AEC result is obtained as

$$\mathcal{F}_{\text{WSTWS}}(Y, X) = Y(t, f) - \hat{\mathbf{h}}_1(t, f)^H \mathbf{X}(t, f), \quad (6)$$

which represents the result of canceling the estimated echo signal from the near-end mixture signal Y based on the far-end signal X . In Eq. (6), $\hat{\mathbf{h}}_1(t, f) \in \mathbb{C}^K$ denotes a K -tap linear filter modeling the echo path, and $\mathbf{X}(t, f) = [X(t, f), X(t-1, f), \dots, X(t-K+1, f)]^T \in \mathbb{C}^K$. In frame-online, real-time AEC, at the current frame t , WSTWS estimates the filter by solving the following problem:

$$\hat{\mathbf{h}}_1(t, f) = \underset{\mathbf{h}_1(f)}{\operatorname{argmin}} \sum_{t'=t-W}^t \frac{|Y(t', f) - \mathbf{h}_1(f)^H \mathbf{X}(t', f)|^2}{\lambda(t, f)}, \quad (7)$$

which is computed based on the current and the past W frames. The weighting term λ is computed as

$$\lambda(t, f) = \varepsilon \times \max_{t' \in [t-W, t]} (|Y(t', f)|^2) + |Y(t, f)|^2, \quad (8)$$

where ε is a floor value to avoid placing too much weight on low-energy T-F units.

3.1.2. Reference signal preprocessing

Although the reference signal contains strong energy of the far-end signal, it still contains a significant amount of near-end signals. To minimize the interference of the near-end components in the reference signal, we first leverage WSTWS to estimate the near-end components and then employ a method similar to real-valued T-F masking [25] to suppress the near-end components. In detail,

$$\hat{M} = \frac{|R - \mathcal{F}_{\text{WSTWS}}(R, X)|}{|R - \mathcal{F}_{\text{WSTWS}}(R, X)| + |\mathcal{F}_{\text{WSTWS}}(R, X)|}, \quad (9)$$

$$R_m = \hat{M}^m \odot R, \quad (10)$$

where $\mathcal{F}_{\text{WSTWS}}(R, X)$ is the WSTWS result calculated based on the reference signal and the far-end signal, $m \in [0, 1]$ is a tunable mask compression factor, and \odot denotes point-wise multiplication. Because the far-end component in the reference signal has dominant energy, Eq. (9) preserves this dominant far-end component. With R_m , we can compute an additional linear AEC result, denoted as $\mathcal{F}_{\text{WSTWS}}(Y, R_m)$, besides using the reference signal R to directly compute a linear AEC result (i.e., $\mathcal{F}_{\text{WSTWS}}(Y, R)$).

3.2. Neural AEC Stage

Fig. 2 illustrates the overall architecture of the proposed AEC model. The network takes 7 input signals: ① far-end signal X , ② near-end mixture signal Y , and ③ reference signal R and ④ its masked version R_m . Additionally, we include the outputs of WSTWS applied to three signal pairs: ⑤ $\mathcal{F}_{\text{WSTWS}}(Y, X)$, ⑥ $\mathcal{F}_{\text{WSTWS}}(Y, R)$, and ⑦ $\mathcal{F}_{\text{WSTWS}}(Y, R_m)$, which respectively represent the linear AEC results between the far-end signal, the reference signal, the masked reference signal, and the near-end mixture signal. This multi-input

design enables the model to leverage complementary echo estimates to improve AEC performance.

To harmonize the heterogeneous input representations and align their temporal dynamics, we apply a dedicated pre-encoding block to the real and imaginary components of each of the seven input signals. Each pre-encoding block consists of a causal 2D convolutional layer with a 3×3 kernel, 2 input channels and 2 output channels, followed by layer normalization [26] and PReLU [27]. The processed features are then concatenated along the channel dimension, resulting in a 14-channel input tensor to the AEC model. The AEC model employs the ICCRN architecture [28]. It is trained to output an estimate of the near-end speech signal, denoted as \hat{S}^d .

3.3. Loss Functions

The loss function combines the two loss functions:

$$\mathcal{L}_{\text{total}} = \mathcal{L}_{\text{RI+Mag}} + \alpha \times \mathcal{L}_{\text{S-SISNR}}, \quad (11)$$

where α is tuned to 0.01. The first loss term, $\mathcal{L}_{\text{RI+Mag}}$, penalizes the complex spectrum as follows:

$$\mathcal{L}_{\text{RI+Mag}} = \mathcal{L}_{\text{RI}} + \mathcal{L}_{\text{Mag}}, \quad (12)$$

$$\mathcal{L}_{\text{RI}} = \sum_{t,f} \left| |S^d(t, f)|^p e^{j\angle S^d(t, f)} - |\hat{S}^d(t, f)|^p e^{j\angle \hat{S}^d(t, f)} \right|^2, \quad (13)$$

$$\mathcal{L}_{\text{Mag}} = \sum_{t,f} \left| |S^d(t, f)|^p - |\hat{S}^d(t, f)|^p \right|^2, \quad (14)$$

where p (tuned to 0.5) is a spectral compression factor following [29]. The second loss term, $\mathcal{L}_{\text{S-SISNR}}$, denotes the stretched scale-invariant signal-to-noise ratio (S-SISNR) loss [30], which is a variant of SISNR [31]. It is a time domain loss function obtained by doubling the period of SISNR:

$$\mathcal{L}_{\text{S-SISNR}} = 10 \log_{10} \cot^2\left(\frac{\beta}{2}\right) = 10 \log_{10} \frac{1 + \cos(\beta)}{1 - \cos(\beta)}, \quad (15)$$

where $\cos(\beta)$ denotes the cosine similarity between the target speech signal s^d and predicted speech signal \hat{s}^d .

4. EXPERIMENTAL SETUP

4.1. Datasets

The near-end and far-end signals employed in our experiments are sourced from the synthetic datasets of the ICASSP 2023 AEC challenge [16] to simulate the near-end and far-end scenarios. The RIRs are generated by using the image method [32]. We simulate different rooms of dimensions $l \times w \times h$, with l randomly sampled from 4 to 8 meters, w from 3 to 7 meters, and h from 3 to 5 meters. The positions of the sound sources (including the loudspeaker and the near-end talker) are randomly set within the room. The auxiliary reference microphones are randomly set within a hollow sphere with a radius of 0.05 to 0.2 meters, centered at the loudspeaker position. The main microphones are randomly placed in the cavity with a length range of $[l/10, l - 1/10]$, a width range of $[w/10, w - w/10]$, and a height range of $[1, \min(h - 1, 3)]$. The reverberation time (T60) is randomly sampled from 0.1 to 0.8 seconds to cover a wide range of acoustic conditions. In total, 22,000 RIRs are generated based on the aforementioned configuration, and 20,000 of them are allocated for training, 1,000 for validation, and 1,000 for testing. The generated echo signal is mixed with near-end speech s at a signal-to-echo

ratio (SER) randomly sampled from the range $[-10, 10]$ dB with a step of 1 dB. We generate a dataset consisting of 100,000 training, 5,000 validation, and 1,000 test mixtures. All samples are 6-second long. The sampling rate is 16 kHz.

4.2. Nonlinearity Scenarios

This study considers five types of nonlinear settings. The first three [33] are used for training. For testing, we construct two test conditions: a matched condition, which employs the first three nonlinear settings, and a mismatched condition, which employs the last two, to verify the effectiveness of introducing auxiliary reference microphones.

$$x_{nl}(n) = \frac{ax(n)}{\sqrt{a^2 + x^2(n)}}, \text{ with } a = \frac{5}{b}, \quad (16)$$

$$x_{nl}(n) = 1 - e^{-ax(n)}, \text{ with } a = \frac{b}{10}, \quad (17)$$

$$x_{nl}(n) = 2ax(n) + ax^2(n) + x^3(n), \text{ with } a = \log\left(\frac{b}{10}\right) + 0.1, \quad (18)$$

where $b \in [2, 5]$. The other two nonlinearities are respectively the combinations of hard-clipping [34] and soft-clipping [35] with sigmoid nonlinearity:

$$x_{\text{hard}}(n) = \begin{cases} -x_{\max}, & x(n) < -x_{\max} \\ x(n), & |x(n)| \leq x_{\max} \\ x_{\max}, & x(n) > x_{\max} \end{cases} \quad (19)$$

$$x_{\text{soft}}(n) = \frac{x(n)x_{\max}}{\sqrt{|x_{\max}|^\rho + |x(n)|^\rho}}, \quad (20)$$

where the clipping threshold x_{\max} is set to 0.7 in this work. For soft-clipping saturation distortion, ρ is set to 2, denoting the non-adaptive shape parameter.

$$x_{\text{sigmoid}}(n) = \lambda \left(\frac{1}{1 + e^{-\nu \cdot z(n)}} - \frac{1}{2} \right), \quad (21)$$

where $z(n) = 1.5 \times x(n) - 0.3 \times x^2(n)$, the parameter λ denotes the sigmoid gain and is set to 2, and ν represents the sigmoid slope and is defined as

$$\nu = \begin{cases} 4, & \text{if } z(k) > 0 \\ 0.5, & \text{if } z(k) \leq 0 \end{cases} \quad (22)$$

For the unmatched test set, the same sound source signals as in the matched test set are used, but with an invisible non-linear setting.

4.3. Training Details

For STFT, the window size is 20 ms, hop size 10 ms, and the Hamming window is used as the analysis window. The model is trained using the Adam optimizer, starting with an initial learning rate of 0.001, which is halved if the validation loss does not improve for 2 epochs. Early stopping is applied if no improvement is observed for 8 epochs. The number of filter taps in WSTWS is tuned to $K = 20$ in default, while in Eq. (9), considering that the loudspeaker and the reference microphone are spatially close to each other, the number of filter taps for WSTWS is tuned to 1. In Eq. (8), the flooring term ε is tuned to 0.001. In Eq. (7), the window size W is tuned to 200 frames. In Eq. (10), the mask compression factor m is tuned 1/6.

Table 1: AEC results on the matched test set.

Test scenarios	DT		ST_NE		ST_FE
	PESQ	SDR (dB)	PESQ	SDR (dB)	ERLE (dB)
Mixture	1.56	-11.8	2.25	-36.1	-
$\mathcal{F}_{\text{WSTWS}}(Y, X)$	1.85	-8.2	-	-	12.4
$\mathcal{F}_{\text{STWS}}(Y, R_m)$	1.76	-7.0	-	-	17.5
$\mathcal{F}_{\text{WSTWS}}(Y, R_m)$	1.88	-8.0	-	-	13.4
ICCRN	2.34	4.1	2.92	5.1	73.5
ICCRN _r	2.37	4.1	2.93	5.3	74.8
ICCRN _{rl}	2.49	4.7	2.96	5.1	73.4
ICCRN _{rl+fl}	2.52	4.7	2.93	5.3	76.1
ICCRN _{rl+fl+mrl}	2.55	5.0	2.95	5.8	77.2
ICCRN_{rl+fl+mrl+w}	2.59	5.1	2.97	5.9	77.8

4.4. Evaluation Setup

We consider three evaluation scenarios, including double talk (DT), near-end single talk (ST_NE), and far-end single talk (ST_FE). Three popular evaluation metrics are used, including echo return loss enhancement (ERLE) [36] for measuring echo suppression during far-end single talk, perceptual evaluation of speech quality (PESQ) [37] for assessing near-end speech quality, and signal-to-distortion ratio (SDR) [38] for quantifying near-end speech fidelity during double talk. The evaluated models consist of linear AEC methods, ICCRN, and ICCRN*. Specifically, the linear AEC methods include $\mathcal{F}_{\text{WSTWS}}(Y, X)$, $\mathcal{F}_{\text{STWS}}(Y, R_m)$, and $\mathcal{F}_{\text{WSTWS}}(Y, R_m)$, while ICCRN* denotes variants that utilize different input features. In detail,

- **ICCRN** uses only the far-end signal and the near-end mixture signal as inputs to predict the target speech.
- **ICCRN_r**, which builds on ICCRN, additionally incorporates the reference signal into its network input.
- **ICCRN_{rl}**, building on **ICCRN_r**, further takes the linear AEC result computed based on the reference signal and the near-end mixture signal as input. It should be noted that the linear AEC result used here is computed based on STWS. That is, $\mathcal{F}_{\text{STWS}}(Y, R)$.
- **ICCRN_{rl+fl}**, building on **ICCRN_{rl}**, further incorporates the STWS result of the near-end mixture signal and the far-end signal. That is, $\mathcal{F}_{\text{STWS}}(Y, X)$.
- **ICCRN_{rl+fl+mrl}**, building on **ICCRN_{rl+fl}**, additionally includes the masked reference signal R_m in Section 3.1.2 and $\mathcal{F}_{\text{STWS}}(Y, R_m)$ to the input signal.
- **ICCRN_{rl+fl+mrl+w}**, building on **ICCRN_{rl+fl+mrl}**, replaces all the STWS operations with WSTWS. The detailed input signals are listed in Section 3.2.

Notice that ICCRN is considered the baseline of the other models, as this is currently the popular way to realize neural AEC.

5. EVALUATION RESULTS

The experimental results on both matched and mismatched test sets demonstrate the effectiveness of the proposed systems.

In Table 1, we observe **ICCRN_{rl+fl+mrl+w}** achieves the best performance across all evaluation metrics on the matched test set. For the DT scenario, it demonstrates a 10.7% improvement in PESQ score (2.59 vs. 2.34) and a 24.3% increase in SDR (5.1 vs. 4.1 dB) compared to the baseline ICCRN. In the ST_NE condition, it attains the highest PESQ score of 2.97 and achieves 5.86 dB SDR, representing a 15.7% improvement over ICCRN. For the ST_FE scenario, it delivers superior echo suppression performance with an ERLE score of 77.8 dB.

Table 2: AEC results on the mismatched test set.

Test scenarios	DT		ST_NE		ST_FE
	PESQ	SDR (dB)	PESQ	SDR (dB)	ERLE (dB)
Mixture	1.52	-12.0	2.28	-36.6	-
$\mathcal{F}_{\text{WSTWS}}(Y, X)$	1.65	-9.0	-	-	7.7
$\mathcal{F}_{\text{STWS}}(Y, R_m)$	1.73	-7.1	-	-	16.8
$\mathcal{F}_{\text{WSTWS}}(Y, R_m)$	1.85	-8.1	-	-	13.4
ICCRN	2.05	3.1	2.92	5.1	36.2
ICCRN _r	2.23	3.7	2.93	5.3	74.0
ICCRN _{rl}	2.10	3.4	2.96	5.1	37.4
ICCRN _{rl+fl}	2.29	4.2	2.98	5.6	65.8
ICCRN _{rl+fl+mrl}	2.38	4.3	2.93	5.6	70.0
ICCRN_{rl+fl+mrl+w}	2.47	4.8	2.97	5.9	72.7

In Table 2, we observe that **ICCRN_{rl+fl+mrl+w}** maintains strong performance in domain-mismatched conditions, demonstrating significant improvements over the baseline ICCRN. In the DT scenario, it achieves a 20.4% higher PESQ score (2.47 vs. 2.05) and a 54.8% enhancement in SDR (4.8 vs. 3.1 dB), highlighting superior speech quality and fidelity. For ST_FE scenario, it sustains a high ERLE score of 72.7 dB, outperforming most variants (except ICCRN_r by 3.9%, which underscores its robust AEC capability even in mismatched conditions.

Introducing the reference signal (ICCRN_r vs. ICCRN) improves ERLE by 37.8 dB (74.0 vs. 36.2 dB) on the mismatched test set, validating the utility of the nonlinear reference signal provided by the auxiliary microphone. Comparisons between ICCRN and ICCRN_{rl+fl} demonstrate the effectiveness of the linear AEC method STWS, which yields significant performance improvements across both matched and mismatched test conditions. Further comparisons between ICCRN_{rl+fl} and ICCRN_{rl+fl+mrl} reveal that linear AEC applied to the purified reference signal also results in notable performance gains. This improvement is particularly pronounced in nonlinear scenario evaluations, as evidenced by the quantitative score differences between $\mathcal{F}_{\text{WSTWS}}(Y, X)$ and $\mathcal{F}_{\text{WSTWS}}(Y, R_m)$. Finally, comparisons between ICCRN_{rl+fl+mrl} and ICCRN_{rl+fl+mrl+w}, alongside those between $\mathcal{F}_{\text{STWS}}(Y, R_m)$ and $\mathcal{F}_{\text{WSTWS}}(Y, R_m)$, confirm that the WSTWS further enhances performance. Collectively, these results validate the model’s strong generalizability and effectiveness in adapting to cross-domain acoustic environments.

6. CONCLUSION

This paper addresses the challenge of nonlinear distortions in AEC, commonly caused by low-cost loudspeakers and amplifiers. We propose a novel AEC framework using an auxiliary reference microphone placed near the loudspeaker to capture nonlinear far-end signals. To suppress near-end speech contamination in the reference microphone signal, we propose a short-time Wiener filtering technique followed by real-valued ratio masking to generate a masked, cleaner reference signal. A weighted STWS module further enhances preliminary suppression before neural processing. Evaluation results show that our method significantly outperforms baselines on both matched and mismatched test sets. It achieves the best performance across all evaluation metrics in matched conditions, and even greater gains (20.4% PESQ and 54.8% SDR) under strong, unseen nonlinearities in double talk scenario. The results demonstrate superior robustness and generalization, validating the effectiveness of introducing an auxiliary reference microphone to help AEC and the STWS-based masking strategy.

7. REFERENCES

- [1] J. Benesty, T. Gänslér *et al.*, “Advances in network and acoustic echo cancellation,” 2001.
- [2] E. Hänsler and G. Schmidt, *Acoustic echo and noise control: a practical approach*. John Wiley & Sons, 2005.
- [3] J. P. Borallo and M. G. Otero, “On the implementation of a partitioned block frequency domain adaptive filter (pbfdaf) for long acoustic echo cancellation,” *Signal Processing*, vol. 27, no. 3, pp. 301–315, 1992.
- [4] N. Bershad and P. Feintuch, “Analysis of the frequency domain adaptive filter,” *Proc. IEEE*, vol. 67, no. 12, pp. 1658–1659, 1979.
- [5] F. Kuech, E. Mabande, and G. Enzner, “State-space architecture of the partitioned-block-based acoustic echo controller,” in *Proc. ICASSP*, 2014, pp. 1295–1299.
- [6] A. Guérin, G. Faucon, and R. Le Bouquin-Jeannès, “Nonlinear acoustic echo cancellation based on Volterra filters,” *IEEE/ACM Trans. Audio, Speech, Lang. Process.*, vol. 11, no. 6, pp. 672–683, 2004.
- [7] T. S. Wada and B.-H. Juang, “Enhancement of residual echo for robust acoustic echo cancellation,” *IEEE Trans. Audio, Speech, Lang. Process.*, vol. 20, no. 1, pp. 175–189, 2011.
- [8] F. Zhao, J. Liu, and X. Zhang, “SDAEC: Signal Decoupling for Advancing Acoustic Echo Cancellation,” in *Proc. Interspeech*, 2024, pp. 172–176.
- [9] G. Zhang, L. Yu, C. Wang, and J. Wei, “Multi-scale temporal frequency convolutional network with axial attention for speech enhancement,” in *Proc. ICASSP*, 2022, pp. 9122–9126.
- [10] C. Zhang, J. Liu, H. Li, and X. Zhang, “Neural Multi-Channel and Multi-Microphone Acoustic Echo Cancellation,” *IEEE/ACM Trans. Audio, Speech, Lang. Process.*, pp. 2181–2192, 2023.
- [11] Z.-Q. Wang, S. Cornell, S. Choi *et al.*, “TF-GridNet: Integrating Full- and Sub-Band Modeling for Speech Separation,” *IEEE/ACM Trans. Audio, Speech, Lang. Process.*, vol. 31, pp. 3221–3236, 2023.
- [12] N. Howard, A. Park, T. Z. Shabestary, A. Gruenstein *et al.*, “A Neural Acoustic Echo Canceller Optimized Using An Automatic Speech Recognizer and Large Scale Synthetic Data,” in *Proc. ICASSP*, 2021, pp. 7128–7132.
- [13] H. Zhao, N. Li, R. Han, L. Chen *et al.*, “A Deep Hierarchical Fusion Network for Fullband Acoustic Echo Cancellation,” in *Proc. ICASSP*, 2022, pp. 9112–9116.
- [14] S. Panchapagesan, A. Narayanan, T. Z. Shabestary, S. Shao *et al.*, “A Conformer-based Waveform-domain Neural Acoustic Echo Canceller Optimized for ASR Accuracy,” *Proc. Interspeech*, 2022, pp. 2538–2542.
- [15] K. Sridhar, R. Cutler, A. Saabas, T. Parnamaa *et al.*, “ICASSP 2021 acoustic echo cancellation challenge: Datasets, testing framework, and results,” in *Proc. ICASSP*, 2021, pp. 151–155.
- [16] R. Cutler, A. Saabas, T. Parnamaa, M. Purin *et al.*, “ICASSP 2023 acoustic echo cancellation challenge,” *IEEE Open Journal of Signal Processing*, vol. 5, pp. 675–685, 2024.
- [17] Z. Chen, X. Xia, S. Sun, Z. Wang *et al.*, “A progressive neural network for acoustic echo cancellation,” in *Proc. ICASSP*, 2023, pp. 1–2.
- [18] Z. Wang, Y. Na, Z. Liu, B. Tian *et al.*, “Weighted recursive least square filter and neural network based residual echo suppression for the AEC-Challenge,” in *Proc. ICASSP*, 2021, pp. 141–145.
- [19] G. Revach, N. Shlezinger, R. J. Van Sloun, and Y. C. Eldar, “Kalmannet: Data-driven kalman filtering,” in *Proc. ICASSP*, 2021, pp. 3905–3909.
- [20] D. Yang, F. Jiang, W. Wu, X. Fang *et al.*, “Low-complexity acoustic echo cancellation with neural Kalman filtering,” in *Proc. ICASSP*, 2023, pp. 1–5.
- [21] Y. Zhang, M. Yu, H. Zhang, D. Yu *et al.*, “Kalmannet: A learnable Kalman filter for acoustic echo cancellation,” *CoRR*, 2023.
- [22] W. Klippel, “Tutorial: Loudspeaker nonlinearities—Causes, parameters, symptoms,” *Journal of the Audio Engineering Society*, vol. 54, no. 10, pp. 907–939, 2006.
- [23] Z.-Q. Wang, G. Wichern, and J. Le Roux, “Convolutional prediction for monaural speech dereverberation and noisy-reverberant speaker separation,” *IEEE/ACM Trans. Audio, Speech, Lang. Process.*, vol. 29, pp. 3476–3490, 2021.
- [24] F. Zhao and X. Zhang, “Attention-Enhanced Short-Time Wiener Solution for Acoustic Echo Cancellation,” in *Proc. ICASSP*, 2025, pp. 1–5.
- [25] A. Narayanan and D. Wang, “Ideal ratio mask estimation using deep neural networks for robust speech recognition,” in *Proc. ICASSP*, 2013, pp. 7092–7096.
- [26] J. L. Ba, J. R. Kiros, and G. E. Hinton, “Layer normalization,” *arXiv preprint arXiv:1607.06450*, 2016.
- [27] K. He, X. Zhang, S. Ren, and J. Sun, “Delving deep into rectifiers: Surpassing human-level performance on imagenet classification,” in *Proc. ICCV*, 2015, pp. 1026–1034.
- [28] J. Liu and X. Zhang, “ICCRN: Inplace Cepstral Convolutional Recurrent Neural Network for Monaural Speech Enhancement,” in *Proc. ICASSP*, 2023, pp. 1–5.
- [29] A. Li, C. Zheng, R. Peng, and X. Li, “On the importance of power compression and phase estimation in monaural speech dereverberation,” *JASA Express Letters*, vol. 1, no. 1, 2021.
- [30] Y. Sun, L. Yang, H. Zhu, and J. Hao, “Funnel Deep Complex U-Net for Phase-Aware Speech Enhancement,” in *Proc. Interspeech*, 2021, pp. 161–165.
- [31] Y. Luo and N. Mesgarani, “Conv-TasNet: Surpassing Ideal Time-Frequency Magnitude Masking for Speech Separation,” *IEEE/ACM Trans. Audio, Speech, Lang. Process.*, vol. 27, no. 8, pp. 1256–1266, 2019.
- [32] J. B. Allen and D. A. Berkley, “Image method for efficiently simulating small-room acoustics,” *The Journal of the Acoustical Society of America*, vol. 65, no. 4, pp. 943–950, 1979.
- [33] C. Zhang, J. Liu, and X. Zhang, “A Complex Spectral Mapping with Inplace Convolution Recurrent Neural Networks For Acoustic Echo Cancellation,” in *Proc. ICASSP*, 2022, pp. 751–755.
- [34] A. Stenger and W. Kellermann, “Adaptation of a memoryless preprocessor for nonlinear acoustic echo cancelling,” *Signal Processing*, pp. 1747–1760, 2000.
- [35] B. S. Nollét and D. L. Jones, “Nonlinear echo cancellation for hands-free speakerphones,” *Proc. NSIP’97*, pp. 8–10, 1997.
- [36] G. Enzner, H. Buchner, A. Favrot, and F. Kuech, “Acoustic echo control,” in *Academic press library in signal processing*. Elsevier, 2014, vol. 4, pp. 807–877.
- [37] A. W. Rix, J. G. Beerends, M. P. Hollier, and A. P. Hekstra, “Perceptual evaluation of speech quality (PESQ)—a new method for speech quality assessment of telephone networks and codecs,” in *Proc. ICASSP*, 2001, pp. 749–752.
- [38] E. Vincent, R. Gribonval, and C. Févotte, “Performance measurement in blind audio source separation,” *IEEE Trans. Audio, Speech, Lang. Process.*, vol. 14, no. 4, pp. 1462–1469, 2006.